Physically Plausible Wrench Decomposition for Multi-effector Object Manipulation

Philine Donner, Satoshi Endo and Martin Buss

Abstract—When manipulating an object with multiple effectors such as in multi-digit grasping or multi-agent collaboration, forces and torques (i.e. wrench) applied to the object at different contact points generally do not fully contribute to the resultant object wrench, but partly compensate each other. The current literature, however, lacks a physically plausible decomposition of the applied wrench into its manipulation and internal components. We formulate the wrench decomposition as a convex optimization problem, minimizing the Euclidean norms of manipulation forces and torques. Physical plausibility in the optimization solution is ensured by constraining the internal and manipulation wrench by the applied wrench. We analyze specific cases of 3digit grasping and 2D beam manipulation, and show the applicability of our method to general object manipulation with multiple effectors. The wrench decomposition method is then extended to quantification of measures important in evaluating physical human-human and human-robot interaction tasks. We validate our approach via comparison to the state of the art in simulation and via application to a human-human object transport study.

Index Terms—Physical Human-Robot Interaction, Grasping, Haptics and Haptic Interfaces, Cooperative manipulators, Force Decomposition, Internal Force

I. INTRODUCTION

EITHER for moving an object or stabilizing it against external force such as gravity, supporting the object from several contact points is often an effective solution in object manipulation. When multiple effectors share the load of a rigid object, a certain object state needs to be attained not only by the force and torque (i.e. wrench) that specify desired manipulation, but also by the wrench compensating those from the other effectors. Decomposition of an applied wrench into *manipulation wrench*, which potentially causes motion, and *internal wrench*[1], which is compensated, is of interest in the present article.

When multiple robotic effectors jointly control an object through rigid grasps, internal wrench is often undesired as it produces stress inside the object [3], [4]. However, a certain level of internal force may be desirable, for example, when sufficient friction has to be generated to securely grasp an

P. Donner and M. Buss are with the Chair of Automatic Control Engineering and the TUM Institute for Advanced Study, Technical University of Munich, Lichtenbergstrasse 2a, 85748 Garching, Germany, e-mail: {philine.donner,mb}@tum.de.

S. Endo is with the Chair of Information-oriented control, Technical University of Munich, Arcisstraße 21, 80290 München, Germany, e-mail: s.endo@tum.de

[1]Note that in mechanics, wrench that exists inside an object and resists external wrench is termed internal wrench, e.g., [1], [2]. Here, we follow the common terminology of the manipulation community and use internal wrench to refer to the compensated external wrench component.

object on a slippery surface [5], [6]. Furthermore, internal wrench can serve as a source for haptic information exchange among decentralized systems such as in physical human-human interaction (pHHI) and human-robot interaction (pHRI) in which control disagreement [7], [8], [9] and action intention [10] need to be understood through the wrench perceived at the interaction. Thus, accurate wrench decomposition is imperative to analyses of multi-effector object manipulation.

In the robotics case, the common approach is to use a pseudoinverse of the grasp matrix to compute the manipulation wrench the effectors need to apply to achieve a desired object state [5], [3], [11]. The grasp matrix relates applied wrench to the resultant wrench acting at the center of mass (CoM) of the object [12]. Internal forces, that lie in the null-space of the grasp matrix and consequently do not influence the object acceleration [13], are added to the manipulation forces according to a task requirement [14], [15]. Kumar and Waldron interpret the difference of forces projected onto the connection lines of the interaction points as internal force. They show that this internal force is zero if the Moore-Penrose pseudoinverse is used to compute applied forces for three fingered grasping [16]. Further extensions of the pseudoinverse wrench decomposition have been successfully used for wrench synthesis, e.g., the virtual linkage model [17] for humanoid robots in complex multi-contact situations [18].

However, such pseudoinverse solutions do not differentiate applied wrench in terms of how it leads to motion or object stress. Yoshikawa and Nagai [19] were among the first to recognize the internal force based on the pseudoinverse solutions does not show how tight an object is grasped. They instead used heuristics for a physically more plausible definition of internal forces in a precision grip, such that forces can only push but not pull. Groten et al. [20] build upon [19] and present force decomposition for the analysis of pHHI and pHRI tasks, though their application is limited to two effectors and one dimensional cases [8].

The lack of a generally applicable wrench decomposition method has let to task specific definitions, with a focus on obtaining, e.g., disagreement measures tailored to the task of interest rather than physically plausible results. In [21], the one dimensional force decomposition solution of [20] was extended to the plane to evaluate a shared control strategy of a mobility assistance robot. Different force decompositions that allow to analyze human five fingered grasping were proposed in [22] and [23]. An alternative, but also task specific approach without physical plausibility considerations was recently presented in [24], where minimum-jerk trajectories were used as a human motion model to decompose applied forces during a simple dyadic object transport task.

An important step towards physically plausible wrench decomposition was recently taken by Schmidts et al. in [25], by introducing force decomposition constraints motivated by mechanical work. The wrench decomposition solution for two effectors proposed in [26] satisfies the proposed constraints of [25]. Erhart and Hirche recently suggested a different decomposition approach for cooperative object manipulation that also includes the application of torque in [27] and is based on kinematic constraint violation of desired accelerations as presented in [28]. One of the main findings of their works is the existence of infinite different pseudoinverses of the grasp matrix that specify desired load shares of the effectors, although their computation of internal wrench does not necessarily comply with the constraints of [25].

In oder to overcome the case specificities and lack of physical plausibility in existing approaches, this study contributes

- an extension of the force constraints proposed by [25] to the application of torque,
- a reformulation of the optimization proposed by [25] based on physical plausibility considerations yielding a convex optimization problem,
- derivation of analytic solutions for special cases
- and wrench measures for analysis of pHRI and pHHI tasks.

The result is a physically plausible wrench decomposition into manipulation and internal components for rigid object manipulation. Our wrench decomposition method extracts internal wrench, for the first time, in a form generalizable to realistic settings such as when quantifying haptic communications in pHHI and pHRI tasks beyond simplified laboratory settings as, e.g., in [10], [29]. The proposed decomposition method is then applied in simulation to validate its results and used to showcase how the method can elucidate underlying coordination strategy in a pHHI behavioural study.

The remainder of this article is organized as follows. In Sec. II, we motivate the need for a physically plausible wrench decomposition by a comparison to the state of the art (SoA) pseudoinverse solutions and formally state our problem. In Sec. III, we formulate physically plausible wrench decomposition as an optimization problem and discuss the solutions for several special cases. Based on the proposed wrench decomposition, we introduce measures for the analysis of pHHI and pHRI tasks in Sec. IV and apply them to simulation examples in Sec. V and a pHHI experiment in Sec. VI. In Sec. VII we discuss limitations and possible extensions of our work. Sec. VIII concludes the article.

II. PROBLEM FORMULATION

In this article, we address the problem of decomposing the wrench applied by n effectors to a rigid object into its motion and internal stress-inducing components in a physically plausible manner.

A. Background

We consider a rigid object as depicted in Fig. 1 with its object-fixed coordinate system $\{o\}$ at the CoM. All vectors
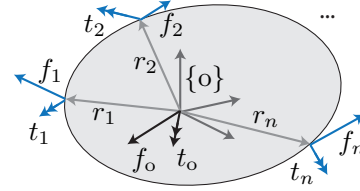

Fig. 1. Rigid object with kinematic quantities: The wrenches $h_i = \begin{bmatrix} f_i^\top & t_i^\top \end{bmatrix}^\top$ with $i = 1, \ldots, n$ are applied at effector positions r_i in the object fixed coordinate system $\{o\}$ and cause a resultant object wrench $h_o = \begin{bmatrix} f_o^\top & t_o^\top \end{bmatrix}^\top$ at the CoM of the object.

throughout this article are given in this coordinate system, unless stated otherwise. Force $f_i \in \mathbb{R}^3$ and torque $t_i \in \mathbb{R}^3$ at the i-th effector position at $r_i \in \mathbb{R}^3$ are combined to the wrench vector $h_i = \begin{bmatrix} f_i^\top & t_i^\top \end{bmatrix}^\top$. The grasp matrix $G \in \mathbb{R}^{6 \times 6n}$ [12] relates the applied wrench $h = \begin{bmatrix} h_1^\top \ldots h_n^\top \end{bmatrix}^\top \in \mathbb{R}^{6n}$ to the resultant object wrench $h_o = \begin{bmatrix} f_o^\top & t_o^\top \end{bmatrix}^\top \in \mathbb{R}^6$ such that

$$h_o = Gh \tag{1}$$

with

$$G = \begin{bmatrix} I_{3\times3} & 0_{3\times3} & \ldots & I_{3\times3} & 0_{3\times3} \\ S(r_1) & I_{3\times3} & \ldots & S(r_n) & I_{3\times3} \end{bmatrix} \tag{2}$$

where $I_{3\times3}, 0_{3\times3} \in \mathbb{R}^{3\times3}$ are identity and zero matrices, and $S(\cdot) \in \mathbb{R}^{3\times3}$ is the skew-symmetric matrix carrying out the cross product operation: $S(a)\, b = a \times b$ [30]. In the following, we refer to the torque induced by the applied force f_i as

$$t_{f,i} = S(r_i)\, f_i \tag{3}$$

and to the resultant torque induced by each effector as

$$t_{o,i} = t_{f,i} + t_i. \tag{4}$$

B. SoA in wrench decomposition

Wrench decomposition refers to splitting the applied wrench h into *manipulation wrench* $h_M = \begin{bmatrix} h_{M,1}^\top \ldots h_{M,n}^\top \end{bmatrix}^\top \in \mathbb{R}^{6n}$ and *internal wrench* $h_I = \begin{bmatrix} h_{I,1}^\top \ldots h_{I,n}^\top \end{bmatrix}^\top \in \mathbb{R}^{6n}$

$$h = h_M + h_I. \tag{5}$$

The compensation wrench lies in the null-space of the grasp matrix, and consequently it does not produce any resultant wrench $0_{6\times1} = Gh_I$. The manipulation wrench h_M is responsible for the resultant object wrench h_o

$$h_o = Gh_M = Gh. \tag{6}$$

The SoA in wrench decomposition is to use a pseudoinverse of the grasp matrix G^+ to compute the manipulation wrench, which yields the decomposition

$$h_{G+,M} = G^+ Gh \quad \text{and} \quad h_{G+,I} = (I_{6n\times6n} - G^+ G)h. \tag{7}$$

The Moore-Penrose pseudoinverse $G^+ = G^\dagger$ yields the minimum norm solution for the manipulation wrench h_M, as used in [14], [17]. The Moore-Penrose pseudoinverse was contrasted with a different "nonsqueezing" pseudoinverse $G^+ = G_\Delta^+$ by Walker et al. in [3], which computes manipulation

wrenches that yield equal effector contributions to the resultant wrench h_{o}.

Alternative approaches have been proposed to endow internal forces f_{I} with a physical meaning. The virtual linkage model by Williams and Khatib proposes to interpret internal forces as the forces that lock virtual prismatic actuators that connect the effectors [17]. Their extension to internal torques that lock virtual spherical joints is a simplification and, as stated in their work, does not lead to a physically plausible decomposition. In [31], on the other hand, internal forces are characterized as the forces that act inside a determinate truss that connects the effectors.

C. Force decomposition in 1D for $n = 2$

As stated in [19], [25], [27], [26] the use of pseudoinverse methods as described above does not allow for a physically plausible wrench decomposition. We illustrate the issues by one dimensional (1D) examples. Consider the beam in Fig. 2(1a) to which $f_1 = 2\,\mathrm{N}$ is applied at the left side but not at the right $f_2 = 0$. The resultant force that accelerates the object is $f_{\mathrm{o}} = 2\,\mathrm{N}$. No force is compensated and f_1 fully contributes to the object acceleration. We thus conclude $f_{\mathrm{M},1} = 2\,\mathrm{N}$ and $f_{\mathrm{M},2} = f_{\mathrm{I},1} = f_{\mathrm{I},2} = 0$ (see Fig. 2(1b)). The solution for the manipulation force in (7), however, equally distributes the resultant wrench $h_{\mathrm{o}} = Gh$ across the effectors through multiplication with the pseudoinverse G^+. For our simple example, (7) yields the same manipulation forces for the Moore-Penrose and the "non-squeezing" pseudoinverse where $f_{G+,\mathrm{M},1} = f_{G+,\mathrm{M},2} = 0.5 f_{\mathrm{o}} = 1\,\mathrm{N}$. The difference to the actually applied wrench h is interpreted as the internal force where $f_{G+,\mathrm{I},1} = -f_{G+,\mathrm{I},2} = 1\,\mathrm{N}$ (see Fig. 2(1c)). Thus, the decomposition is physically implausible; although no force is applied at r_2, this decomposition method claims that a force of $f_{G+,\mathrm{I},2} = -1\,\mathrm{N}$ at r_2 is compensated.

Fig. 2(2,3) show two additional examples of applied forces that lead to the same resultant force $f_{\mathrm{o}} = 2\,\mathrm{N}$. From the examples in Fig. 2, we observe:

- the pseudoinverse solutions decompose applied forces based on the assumption of fixed equal load shares and thus yield internal force $f_{\mathrm{I},i} \neq 0$ whenever $f_i \neq 0.5 f_{\mathrm{o}}$
- a physically plausible force decomposition should only yield nonzero internal force, when forces are applied into opposing directions, e.g., $f_{\mathrm{I},2} = -f_{\mathrm{I},1} = -1\,\mathrm{N}$ (Fig. 2(3)). Different load shares (Fig. 2(1,2)) that do not lead to force compensation should yield zero internal forces $f_{\mathrm{I},i} = 0$.

Based on the above observations, we propose analogously to [20] to compute internal forces in 1D for effectors $i = 1, 2$ by

$$f_{\mathrm{I},i} = \frac{1}{2}\,\mathrm{sgn}(f_i)(|f_1| + |f_2| - |f_1 + f_2|). \qquad (8)$$

Note that, for wrench synthesis, the Moore-Penrose pseudoinverse $G^\dagger$ yields desired wrenches $h^{\mathrm{d}} = G^\dagger h_{\mathrm{o}}^{\mathrm{d}}$ for given desired resultant wrenches $h_{\mathrm{o}}^{\mathrm{d}}$ which result in zero internal wrenches $h_{\mathrm{I}} = 0$. The main drawback of $G^\dagger$ is the fixed load shares among effectors which do not allow for a physically plausible analysis of measured wrench h. As shown in [27]

for a simple example, the "nonsqueezing" pseudoinverse G_Δ^+ can yield desired wrenches h^{d} that are not free of internal wrenches $h_{\mathrm{I}} \neq 0$. Erhart and Hirche derive a parametrized pseudoinverse that represents infinite different load shares that will yield zero internal wrench [27]. Based on the Gauss' principle, they compute applied effector wrenches given desired effector accelerations and object and effector kinematics and dynamics. Motivated by the reasoning that internal wrench occurs whenever desired effector accelerations violate kinematic constraints, they propose to compute internal wrench similarly to the effector wrenches in [27], but by exclusively considering the effector constraints [4]. However, the internal wrench computation in [4] yields results that differ from our proposed physically plausible wrench decomposition[2].

D. Problem statement for physically plausible wrench decomposition

Internal wrench is defined to lie in the null space of the grasp matrix. Thus, the virtual work by the internal wrench h_{I} needs to be zero for any virtual displacement of the object [13] or of the effectors that satisfy the kinematic constraints [27]. We agree with above definitions but add further restrictions for physical plausibility through the following definition of internal wrench h_{I}

Definition 1. *A physically plausible internal wrench h_{I} lies in the null space of the grasp matrix $0_{6 \times 1} = Gh_{\mathrm{I}}$ and the components $h_{\mathrm{I},i}$ of the effectors $i = 1, \ldots, n$ obey the constraints*

$$\left\| f_{\mathrm{I},i} \right\| \ \leq \ f_i^\top \frac{f_{\mathrm{I},i}}{\left\| f_{\mathrm{I},i} \right\|}, \qquad (9)$$

$$\left\| t_{f\mathrm{I},i} \right\| \ \leq \ t_{f,i}^\top \frac{t_{f\mathrm{I},i}}{\left\| t_{f\mathrm{I},i} \right\|}, \qquad (10)$$

$$\left\| t_{\mathrm{I},i} \right\| \ \leq \ t_i^\top \frac{t_{\mathrm{I},i}}{\left\| t_{\mathrm{I},i} \right\|}, \qquad (11)$$

where $\left\| \cdot \right\|$ denotes the Euclidean norm.

Fig. 3 illustrates the implications of above definition in 2D for applied force f_i. Let the applied force f_i in Fig. 3(a) be not fully contributing to the resultant object acceleration, but partly compensated by an opposing force. Here, we illustrate the opposing force by an ideal linear spring, which can only generate opposing forces along its axis a. The Euclidean norm of internal force $f_{\mathrm{I},i}$ is then upper bounded by the projection of the applied wrench f_i onto a in negative direction

$$\left\| f_{\mathrm{I},i} \right\| \ \leq \ -f_i^\top a, \qquad (12)$$

with $f_{\mathrm{I},i}$ and its corresponding $f_{\mathrm{M},i}$ enclosing an angle $\geq 90\,\mathrm{deg}$. Variation of the direction of a changes the direction of possible compensation, as illustrated in Fig. 3(b).

---

[2]Consider the example displayed in Fig. 2(1a) wherein desired effector accelerations $\ddot{x}_1^{\mathrm{d}} = \frac{8}{3}\,\mathrm{m/s^2}$ and $\ddot{x}_2^{\mathrm{d}} = \frac{4}{3}\,\mathrm{m/s^2}$, effector masses $m_1 = m_2 = 1\,\mathrm{kg}$ and object mass $m_{\mathrm{o}} = 1\,\mathrm{kg}$ result in applied forces $f_1 = 2\,\mathrm{N}$ and $f_2 = 0$. However, internal wrench computed according to [4] yields $f_{\mathrm{I},2} = -f_{\mathrm{I},1} = -\frac{2}{3}\,\mathrm{N}$. Thus, the internal force $f_{\mathrm{I},2}$ exceeds the applied force f_2. See [27], [4] for details.
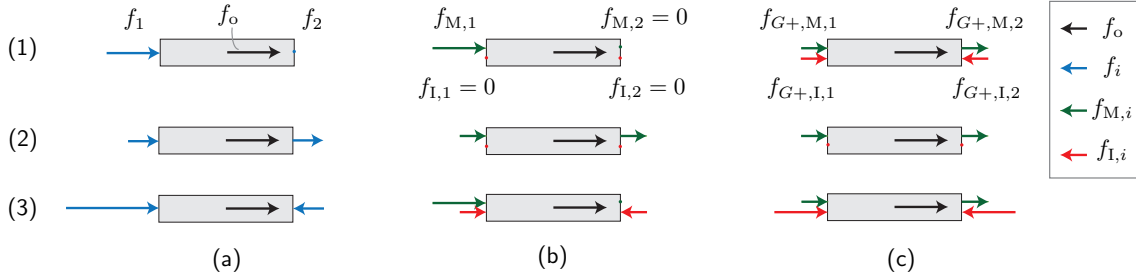
Fig. 2. 1D examples to illustrate the problem of wrench decomposition based on pseudoinverses: (1) Effector 1 (left) takes over the complete load $f_1 = f_o$, (2) effector 1 and 2 equally share the load, (3) effector 2 applies an opposing force that is compensated. (a) Applied forces f_i and resultant object force f_o, (b) physically plausible wrench decomposition with manipulation forces $f_{M,i}$ and internal forces $f_{I,i}$, (c) wrench decomposition based on pseudoinverses with fixed load share yields manipulation forces $f_{G+,M,1} = f_{G+,M,2} = 0.5 f_o$ and internal forces $f_{G+,I,i} = f_i - f_{G+,M,i}$ with $i = 1, 2$.
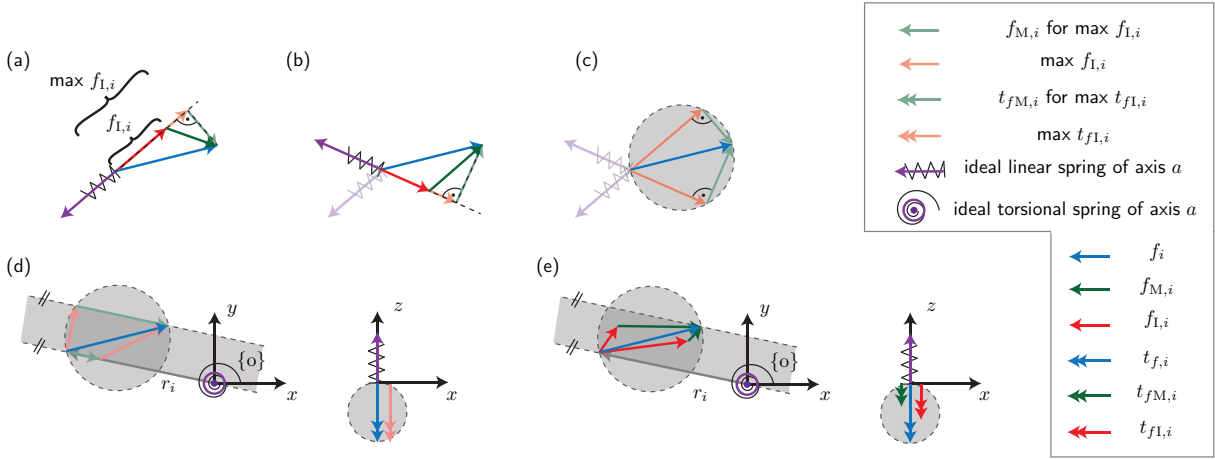
Fig. 3. Illustration of physically plausible internal force in 2D: (a,b) Linear springs of axis a partly compensate applied force f_i in two different directions. (c) Variation of compensation axis a yields to the circular constraint for physically plausible internal force $f_{I,i}$. The decompositions for maximum compensation along the axes in (a) and (b) are inscribed. (d,e) Torsional spring with axis a compensates torque $t_{f,i}$ (right) induced by applied force f_i (left). Two different example decompositions where the torque induced by f_i is (d) completely compensated ($t_{f,iz} = t_{fI,iz}$) and (e) partly compensated, but to the same extent ($|t_{f,iz}| > |t_{fI,iz}|$). The restriction that internal torque cannot exceed the torque induced by f_i yields a band parallel to r_i as additional constraint in 2D force space, which is equivalent to a circular constraint in 2D torque space. 1D torque arrows along z are shown side by side for better visibility.

All directions of a have in common that for maximum compensation, i.e. maximum Euclidean internal force norm $\|f_{I,i}\|$, the internal force $f_{I,i}$ and its corresponding manipulation force $f_{M,i}$ enclose a 90 deg angle. Consequently, all physically plausible force decompositions of f_i are bounded by the dashed circle inscribed in Fig. 3(c). In 3D, the circular constraint extends to a sphere. As compensation can only occur in along the opposite direction of a, we can replace a with the negative normalized internal force $a = -f_{I,i} \|f_{I,i}\|^{-1}$ in (12) and obtain the constraint (9). The force inequality in (9) was first introduced by [25]. In Appendix A, we show that although the proposed circular constraint is required for a physically plausible wrench decomposition, it does not obey work constraints as stated in [25].

Fig. 3(d) and (e) show 2D examples for constraint (10) with respect to force induced torque. Force f_i (left) results in a torque $t_{f,i}$ at the CoM around the negative z-axis (right), which again does not fully contribute to the resultant object acceleration, but is fully (d) or partly (e) compensated by an opposing torque. The opposing torque is illustrated by an ideal torsional spring with axis a such that the torsional spring can only generate opposing torque around its axis a. The Euclidean

norm of the internal torque $t_{fI,i}$ is upper bounded by the projection of the applied force induced torque $t_{f,i}$ onto a in negative direction

$$\|t_{fI,i}\| \leq -t_{f,i}^\top a. \tag{13}$$

For the 2D cases in Fig. 3(d) and (e), this results in an additional constraint: the band constraining the internal force $f_{I,i}$ such that it cannot induce a higher torque around the negative z-axis than the applied force f_i can induce. In 3D the constraint forms a cylinder spanned by the vector r_i and the applied force f_i in force space. In torque space, the constraint for force induced torque is a circle in 2D and a sphere in 3D. As torque compensation can only occur around the opposite direction of a, we replace a with the normalized internal torque $a = -t_{fI,i} \|t_{fI,i}\|^{-1}$ in (13), and obtain constraint (10). Analogously, constraint (11) for internal torque $t_{I,i}$ can be derived, which forms a circle in 2D and a sphere in 3D.

Complementary to Definition 1, we can also define physically plausible manipulation wrench.

Definition 2. *A physically plausible manipulation wrench h_M achieves the object wrench $h_o = G h_M$ and the components*

$h_{M,i}$ of the effectors $i = 1, \ldots, n$ obey the constraints

$$\left\| f_{M,i} \right\| \leq f_i^\top \frac{f_{M,i}}{\left\| f_{M,i} \right\|}, \tag{14}$$

$$\left\| t_{fM,i} \right\| \leq t_{f,i}^\top \frac{t_{fM,i}}{\left\| t_{fM,i} \right\|}, \tag{15}$$

$$\left\| t_{M,i} \right\| \leq t_i^\top \frac{t_{M,i}}{\left\| t_{M,i} \right\|}, \tag{16}$$

where $\left\| \cdot \right\|$ denotes the Euclidean norm.

Proposition 1. *The constraints* (9)-(11) *are equivalent to constraints* (14)-(16).

Proof. See Appendix B. $\qquad \square$

Fig. 4 illustrates the implications of the manipulation based physical plausibility definition in 2D for applied force f_i.

Within the null space of the grasp matrix G, Definition 1 and equivalently Definition 2, further restrict the internal wrench solutions to obey $3n$ constraints for physical plausibility. Still, infinite wrench decomposition solutions exist. As we are interested in decomposing applied wrench into manipulation wrench h_M, which is necessary to produce the resultant object wrench h_o, and the part of the applied wrench, which was compensated h_I, we formulate our problem as follows.

Problem 1. *Decompose a given applied wrench h into manipulation wrench h_M and internal wrench h_I for a given grasp matrix G with $h = h_M + h_I$, such that the manipulation wrenches $h_{M,i}$ applied by effectors $i = 1, \ldots, n$ represent a set of forces and torques of minimum Euclidean norm required to achieve a resultant object wrench $h_o = Gh$, and such that the internal wrench h_I and the manipulation wrench h_M are physically plausible according to Definition 1 and Definition 2, respectively.*

III. WRENCH DECOMPOSITION AS AN OPTIMIZATION PROBLEM

We propose that the solution to Problem 1 can be formulated as a convex scalarized multi-objective optimization that minimizes a manipulation wrench h_M dependent cost function J for a given applied wrench h

minimize

$$J = \sum_{i=1}^n \left(1 - w\right) \left\| f_{M,i} \right\| + sw \left\| t_{fM,i} \right\| + w \left\| t_{M,i} \right\| \tag{17}$$

subject to

$$Gh_M = Gh, \tag{18}$$
$$f_{M,i}^\top f_{M,i} \leq f_i^\top f_{M,i}, \tag{19}$$
$$t_{fM,i}^\top t_{fM,i} \leq t_{f,i}^\top t_{fM,i}, \tag{20}$$
$$t_{M,i}^\top t_{M,i} \leq t_i^\top t_{M,i}, \tag{21}$$
$$i = 1, \ldots, n,$$

where $s = \{0, 1\}$ includes or excludes the manipulation torques induced through forces $t_{fM,i}$ (3) in the cost J. The scalarized multi-objective cost function J yields the Pareto-optimal points associated with a weighting $w \in \,]0, \, 1[$ between

the objectives of Euclidean norm minimization of manipulation forces and torques [32]. As forces and torques are of different units, a plausible weighting w must be selected. The choice of including ($s = 1$) or excluding ($s = 0$) the force induced torque $t_{fM,i}$ in the cost function relates to this issue. We discuss the effects of weighting w and selection parameter s in the following subsections in greater detail.

The inequality constraints (19)-(21) ensure a physically plausible decomposition as stated formally in the following Theorem.

Theorem 1. *A physically plausible wrench decomposition according to Definition 1 must obey the inequality constraints* (19)-(21).

Proof. See proof of Proposition 1 in Appendix B with intermediate result (37). $\qquad \square$

The computation of a physically plausible force decomposition has been written as an optimization problem in [25], but as a non-convex maximization of internal force $J = f_I^T f_I$ with $f_I = \begin{bmatrix} f_{I,1}^\top \ldots f_{I,n}^\top \end{bmatrix}^\top$ subject to the inequality constraint (19). Based on Definition 1, we complete the force constraints by also considering force induced torque through inequality constraint (20). Inequality constraint (21) further extends the constraints to the application of torques. In summary, a total of $3n$ inequality constraints must be met for a physically plausible wrench decomposition according to Problem 1.

For some special cases, maximization of internal wrench $J = h_I^T h_I$ as proposed in [25] and minimization of manipulation wrench according to (17), both subject to constraints (18)-(21), yield the same solution. However, as we show by our examples in the following subsections, maximization of $J = h_I^T h_I$ does not generally comply with Problem 1.

The complexity of the convex optimization problem defined in (17)-(21) rises with the number of effectors n. However, analytic solutions can be found for some special cases as presented in the following.

A. Special case: a point mass

Proposition 2. *The optimization problem* (17)-(21) *has the following analytical solutions for a point mass*[3]

$$f_{M,i} = \theta_{f,i} \max\left(\frac{f_i^\top f_o}{\left\| f_o \right\|^2}, 0\right) f_o, \quad t_{M,i} = \theta_{t,i} \max\left(\frac{t_i^\top t_o}{\left\| t_o \right\|^2}, 0\right) t_o, \tag{22}$$

with $\theta_{f,i} \in [0, 1]$ and $\theta_{t,i} \in [0, 1]$ such that $f_o = \sum f_{M,i}$ and $t_o = \sum t_{M,i}$, independent of s, w in (17).

Proof. See Appendix C. $\qquad \square$

Fig. 5(a) and (b) illustrate the point mass solution for forces f_i applied by three effectors $i = 1, 2, 3$. The same holds for torques. The weighting factor $\theta_{f,i}$ in (22) determines the extent to which projected forces $f_{f_o\|,i}$ pointing into the same direction as the resultant force f_o belong to manipulation force. Infinite solutions for $\theta_{f,i}$ can lead to the same cost J, e.g.,

[3]With the term point mass we refer to the case $t_{f,i} = S(r_i) \, f_i = 0_{3\times1}$ for $i = 1, \ldots, n$. The solution is independent of the actual mass and moment of inertia properties.
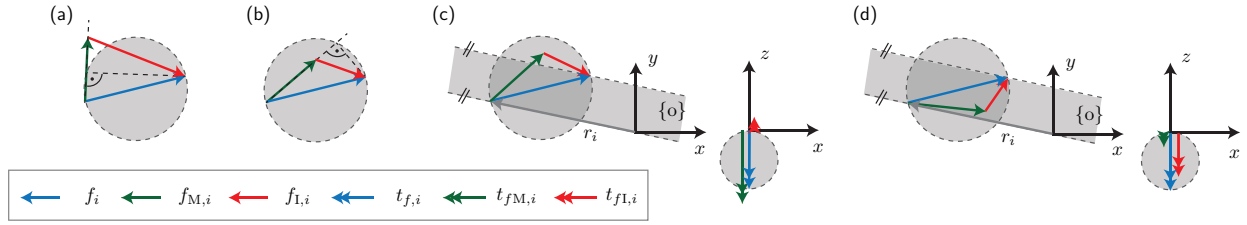
Fig. 4. Illustration of physically plausible manipulation force in 2D: Examples for physically implausible (a,c) and plausible (b,d) force decompositions. (a) The manipulation force $f_{M,i}$ violates the circular force constraint, i.e. the linear acceleration produced by $f_{M,i}$ is not attainable by the applied force f_i; the Euclidean norm of the manipulation force $f_{M,i}$ exceeds the projection of the applied force f_i onto the manipulation force $f_{M,i}$. (c) The manipulation force $f_{M,i}$ violates the band shaped force induced torque constraint, i.e. the rotational acceleration of the object {o} produced by manipulation force $f_{M,i}$ (force induced torque $t_{fM,i}$) is not attainable by the applied force f_i (force induced torque $t_{f,i}$): $\|t_{fM,i}\| > \|t_{f,i}\|$.
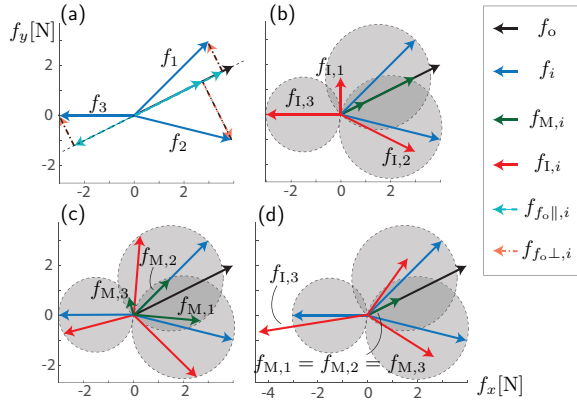

Fig. 5. Point mass example $n = 3$: (a,b) Minimization of manipulation wrench (17). Projections onto the resultant force $f_{f_o\|,i}$ represent maximum possible contributions to f_o and, thus, potential manipulation force $f_{M,i}$. Components $f_{f_o\|,i}$ that point into the opposite direction of f_o and perpendicular components $f_{f_o\perp,i}$ belong to internal force. Thus, $f_{I,3} = f_{f_o\|,3} + f_{f_o\perp,3} = f_3$. (c) Maximization of $J = f_I^\top f_I$ leads to manipulation forces that are not parallel to the resultant force f_o and consequently to manipulation forces of greater Euclidean norm than necessary. (d) Pseudoinverse based decomposition with $G^+ = G^\dagger = G_\Delta^+$ for point masses result in equal manipulation forces for all effectors that violate the force constraints. Only (a,b) represents a physically plausible wrench decomposition according to Problem 1.

the resultant force $f_o = [4 \quad 2 \quad 0]^\top$ can be formed through manipulation forces $f_{M,1} = [2 \quad 1 \quad 0]$ and $f_{M,2} = [2 \quad 1 \quad 0]$ or through $f_{M,1} = [3 \quad 1.5 \quad 0]$ and $f_{M,2} = [1 \quad 0.5 \quad 0]$ (displayed in Fig. 5(b)). A parsimonious selection for $\theta_{f,i} = \theta(x = f_{f_o\|})$ from an analysis point of view is

$$\theta(x) = 1 - \frac{A_x - B_x}{A_x + B_x}, \quad A_x = \sum_{i=1}^{n} \|x_i\|, \quad B_x = \left\|\sum_{i=1}^{n} x_i\right\| \tag{23}$$

which yields $\|f_{M,i}\| \propto \|f_{f_o\|,i}\|$ for same direction of $f_{f_o\|,i}$ and f_o. Note that $\theta(x = f_{f_o\|})$ is equal for all effectors.

Fig. 5(c) displays the solution for a maximization of internal force $J = f_I^\top f_I$ as proposed in [25] also subject to (18)-(21). The cost function $J = f_I^\top f_I$ leads to solutions on the circular force constraints, with the effect that the summed Euclidean norms are not only greater for internal force $\sum_{i=1}^{3} \|f_{I,i}\| = 9.69\,\text{N}$, but also for manipulation force $\sum_{i=1}^{3} \|f_{M,i}\| = 5.58\,\text{N}$ compared to the manipulation wrench based cost (17), $\sum_{i=1}^{3} \|f_{I,i}\| = 7.85\,\text{N}$ and $\sum_{i=1}^{3} \|f_{M,i}\| = 4.47\,\text{N}$. Thus, the force decomposition components are of greater Euclidean
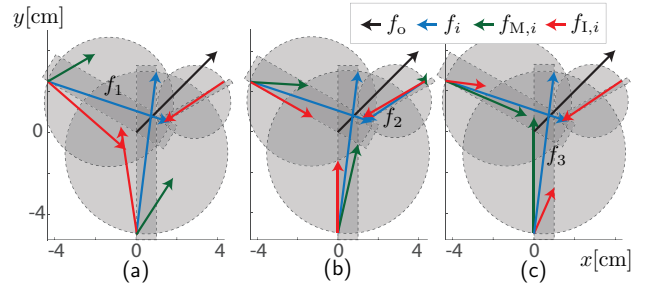

Fig. 6. Three fingered grasping example $n = 3$: (a) Result from [19] violates the constraints for force induced torque. Manipulation forces $f_{M,1}$ and $f_{M,2}$ induce torques of higher Euclidean norm than the applied forces f_1 and f_2. (b) Result for cost (17) $s = 1$, $w = 0.001$ and $s = 0$. (c) Result for cost (17) $s = 1$, $w = 0.5$ and $w = 0.999$. For $s = 1$, increasing weighting w shifts the results from sum of $\|f_{M,i}\|$ minimization to sum of $\|t_{fM,i}\|$ minimization. Length of force arrows $1\,\text{cm} \hat{=} 1\,\text{N}$.

norm than necessary, which conflicts with Problem 1. It also indicates that the approach proposed by Schmidts et al. did not achieve its goal of finding a decomposition free of "virtual forces" [25]. Hence, this example illustrates a rationale for minimization of the cost function based on manipulation wrench (17). Fig. 5(d) shows the pseudoinverse force decomposition results which are physically implausible according to Definition 1; the Euclidean norm of the internal force $\|f_{I,3}\|$ exceeds the Euclidean norm of the applied force $\|f_3\|$.

The wrench decomposition of [26] is equivalent to (22) for $n = 2$ and if forces do not produce torque, i.e. $t_{f,i} = 0$. In [26], the point mass decomposition is also used when force does produce torque, i.e. $t_{f,i} \neq 0$, by inserting $t_{o,i} = t_i + t_{f,i}$ for t_i in (22). We refer to this decomposition as "point mass approximation" in the following.

B. Special case: three-fingered grasping

Fig. 6 displays an example presented in [19] for a three-fingered grasp. Frictional point contact was assumed, such that each finger only applies force, but no torque. Fig. 6(a) shows that the force decomposition based on the heuristics given in [19] violates the force constraints for force induced torque (20). Fig. 6(b) and (c) show optimization solutions according to (17)-(21). While for $s = 0$ the cost does not include torque and consequently the solution is independent of weighting w, for $s = 1$ weighting has an effect. Based on
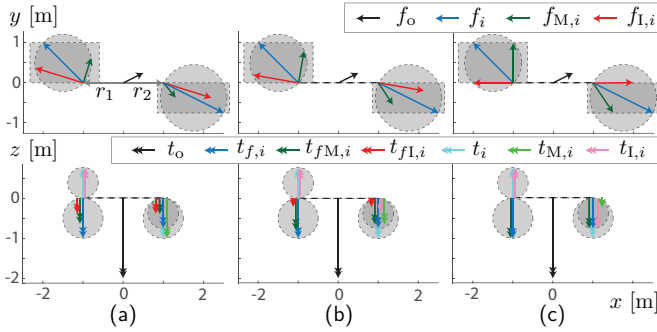
Fig. 7. Beam example $n = 2$ for special case with s, w dependent solution: Results for cost (17) with (a) $s = 0$, $w = 0.001$ and $s = 1$, $w \in \mathbb{R}^+$, (b) $s = 0$, $w = 0.5$, (c) $s = 0$, $w = 0.999$ and the analytical "prioritized torque through torque compensation" (pTtTC) solution. For $s = 0$, increasing w shifts the results from torque through force compensation ($t_{I,2} = 0$) and sum of $\left\| f_{M,i} \right\|$ minimization to torque through torque compensation ($t_{fI,1} = t_{fI,2} = 0$) and sum of $\left\| t_{M,i} \right\|$ minimization. Length of force and torque arrows $1\,\mathrm{m} \hat{=} 1\,\mathrm{N}$ and $1\,\mathrm{m} \hat{=} 1\,\mathrm{Nm}$.

Fig. 8. 3D example decomposition for $n = 3$: Forces (left, $1\,\mathrm{m} \hat{=} 1\,\mathrm{N}$) and torques (right, $1\,\mathrm{m} \hat{=} 1\,\mathrm{Nm}$) with spherical force and torque constraints, (19) and (21). The force induced torque constraints (20) are cylinders in force space (left) and spheres in torque space (right).

the results of Fig. 6(b) and (c), we recommend to set $s = 0$. Intuitively, it makes more sense to minimize the Euclidean norms of force that need to be applied than accepting forces of higher Euclidean norms as long as these forces have a minimum effect on torque production.

C. Special case: a 2D beam

We consider a beam as displayed in Fig. 2 as a 2D special case for two effectors applying forces in the x/y-plane and torque around the z-axis $h_i = \begin{bmatrix} f_{ix} & f_{iy} & 0_{1 \times 3} & t_{iz} \end{bmatrix}^\top$, $i = 1, 2$. For the 2D case, analytic solutions equal for all $s \in \{0, 1\}$ and $w \in]0, 1[$ can be found, by dividing the problem into cases according to the signs and magnitudes of applied forces and torques, e.g., $t_{I,iz} = 0$ if $\mathrm{sgn}(t_{iz}) = \mathrm{sgn}(t_{f,1z}) = \mathrm{sgn}(t_{f,2z})$ for $i = 1, 2$, where $t_{f,1z}$ is the torque around the z-axis caused by applied force f_1. Only one special case requires optimization

$$\{ h \in \mathbb{R}^{12} | (\mathrm{sgn}(t_{f,1z}) = \mathrm{sgn}(t_{f,2z}) = \mathrm{sgn}(t_{kz}) \neq \mathrm{sgn}(t_{jz}))$$
$$\wedge (|2t_{fI,\mathrm{max}z} + t_{kz}| > |t_{jz}|) \, \forall k, j \in \{1, 2\}, k \neq j \}, \quad (24)$$

where $t_{fI,\mathrm{max}z} = \min(t_{f,1z}, t_{f,2z})$. An example for this case is displayed in Fig. 7. The torque applied by effector 1 (t_1) is fully compensated. However, the allocation of $t_{I,1}$ to $t_{I,2}$, $t_{fI,1}$ and $t_{fI,2}$ requires optimization. The results for this optimization differ based on the cost function parameters s and w. In contrast to the three fingered grasping example, $s = 1$ yields results independent of weighting w, while for $s = 0$ weighting w affects the solution (see Fig. 7(b,c)). The solution for $s = 0$ and $w \to 1$ can be found analytically with the advantage such that the wrench decomposition does not require any optimization and it is suitable for real-time applications. We refer to this case as "prioritized torque through torque compensation" (pTtTC).

Based on our conclusions from the grasping example of the previous section and the need for a meaningful measure for analysis, we recommend to use the cost function (17) with $s = 0$, $w = 0.5$. However, in some tasks, the efficient pTtTC can yield results that 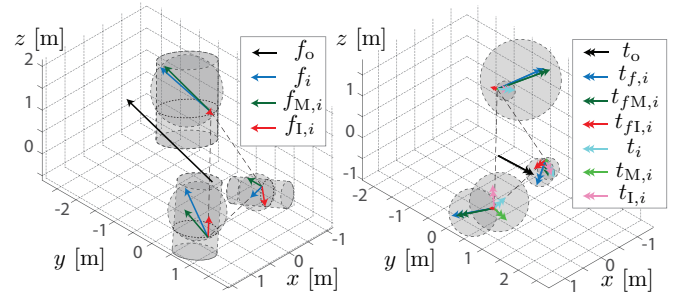are almost equal to the optimization with $s = 0$, $w = 0.5$. Details on the analytic 2D beam solutions and their *MATLAB* implementation can be found in the Multimedia Attachment.

D. General rigid objects

The optimization (17)-(21) decomposes applied wrenches of any number of effectors n located at any position r_i with $i = 1, \ldots, n$. For general rigid bodies, the solutions are weighting dependent for $s = 0$ and $s = 1$. The effect of w can be summarized as follows:

- $\sum_{i=1}^{n} \left\| f_{M,i} \right\|$ increases with increasing w for $s = \{0, 1\}$
- $\sum_{i=1}^{n} \left\| t_{M,i} \right\|$ decreases with increasing w for $s = \{0, 1\}$, stronger decrease for $s = 0$
- $\sum_{i=1}^{n} \left\| t_{fM,i} \right\|$ decreases with increasing w for $s = 1$

Fig. 8 shows a 3D wrench decomposition example for 3 effectors based on cost (17) with $s = 0$ and $w = 0.5$.

IV. MEASURES FOR ANALYSIS

In the following, we present applications of the wrench decomposition for analysis in pHRI and pHHI tasks based on our derivations in the previous sections.

A. Load share

The *load share* parameter $\alpha_{f,i}$ ($\alpha_{t,i}$) describes the fraction of force (torque) contributed by effector i to the resultant force f_o (torque t_o) and can be computed as

$$\alpha_{f,i} = \theta_{f,i} \max(\frac{f_i^\top f_o}{\left\| f_o \right\|^2}, 0), \quad \alpha_{t,i} = \theta_{t_o,i} \max(\frac{t_o^\top t_o}{\left\| t_o \right\|^2}, 0), \quad (25)$$

where the force load share $\alpha_{f,i}$ is equivalent to the point mass solution in (22) with $\theta_{f,i} = \theta(x = f_{f_o\|})$ in (23). The torque load share $\alpha_{t,i}$ also considers torque induced through forces with $\theta_{t,i} = \theta(x = t_{o,t_o\|})$ in (23), where $t_{o,t_o\|,i}$ is the projection of $t_{o,i}$ in (4) onto the resultant torque t_o. Note that $\sum_{i=1}^{n} \alpha_{f,i} = \sum_{i=1}^{n} \alpha_{t,i} = 1$.

Above load shares were introduced in [26] for $n = 2$. The force load share $\alpha_{f,i}$ is related to the weighting introduced in [33] for precise object positioning and to the assistance level in shared control for pHRI [34]. For the 1D case and two effectors, Groten et al. [20] computed the force load

share as $\alpha_{f,i} = \frac{f_{M,i}}{f_o}$. For the general 3D case, we cannot use the manipulation force $f_{M,i}$ and torque $t_{o,M,i}$ at the CoM to compute load share, but we need to relate applied forces to the CoM as in (25). This is due to the fact that manipulation wrench h_M still contains parts that can cancel on force or torque level (see for example Fig. 6 and 7).

B. Energy share

In addition to above load share, the energy transfer among the effectors and the object can be of interest (see, e.g., [35] for a 1D analysis). For a lossless system, the change in object energy is equal to the sum of the agents' energy flows $\dot{E}_o = \sum_{i=1}^{n} \dot{E}_i$. Agent i can cause a change in translational and rotational energy $\dot{E}_i = \dot{E}_{\text{lin},i} + \dot{E}_{\text{rot},i} = f_i^\top \dot{p}_o + t_{o,i}^\top \omega_o$. The energy flow transferred between the agents, without influencing the object energy E_o, can be calculated similarly to internal forces in the 1D case (8) $\dot{E}_I = \frac{1}{2}(\sum_{i=1}^{n} |\dot{E}_i| - |\sum_{i=1}^{n} \dot{E}_i|)$. Similar to the load share, we define the parameter *energy share* of effector i for the complete energy flow

$$\beta_i = \theta_{\dot{E},i} \max(\frac{\dot{E}_i}{\dot{E}_o}, 0), \qquad (26)$$

and for rotational and translational energy flows

$$\beta_{\text{lin},i} = \theta_{\dot{E}\text{lin},i} \max(\frac{\dot{E}_{\text{lin},i}}{\dot{E}_{\text{lin},o}}, 0), \ \beta_{\text{rot},i} = \theta_{\dot{E}\text{rot},i} \max(\frac{\dot{E}_{\text{rot},i}}{\dot{E}_{\text{rot},o}}, 0), \qquad (27)$$

with $\theta_{\dot{E}(\text{lin}/\text{rot}),i} = \theta(x = \dot{E}_{(\text{lin}/\text{rot})})$ in (23).

C. Disagreement

Internal wrench can indicate disagreement [7], [8], [36] and allow to communicate intention through the haptic channel [10]. However, previous works were limited to 1D cases. In order to compare internal wrench within a trial or among different trials, the sum of Euclidean norms of internal force and torque can serve as a measure of disagreement in translational and rotational directions

$$F_I = \frac{1}{2} \sum_{i=1}^{n} \|f_{I,i}\|, \qquad T_I = \frac{1}{2} \sum_{i=1}^{n} \|t_{o,I,i}\|. \qquad (28)$$

As a combined measure for translation and rotation, we propose the measure *relative cost* γ

$$\gamma = 1 - \frac{J(h_M)}{J(h)}. \qquad (29)$$

The cost function (17) is evaluated twice, once at its minimum $J(h_M)$ and another at its maximum $J(h)$. The relative cost returns values $\gamma \in [0, 1]$, where $\gamma = 1$ signifies maximum disagreement, i.e. $h_o = 0_{6x1}$ and $h = h_I$, and $\gamma = 0$ signifies no disagreement in the sense that the complete applied wrench was needed to produce the resultant wrench h_o, i.e. $h = h_M$. The need for an interpretable measure γ strengthens our recommendation not to choose extreme values for w but rather $w = 0.5$ and $s = 0$.

V. ANALYSIS OF SIMULATED MANIPULATION TASKS

In real pHHI and pHRI tasks, the internal state of human agents (i.e. the control disagreement) cannot be precisely and systematically controlled, and the lack of ground truth impedes an interpretation of the results. Thus, we first use simulations to evaluate the proposed method, and assess the quality of the wrench decomposition solutions, before we apply them to a real pHHI task in Sec. VI. Based on the relevant use cases discussed in the introduction, we chose two different simulation scenarios: shared control of a mobility assistance robot [21] and an object transport task [24], [26]. For multi-digit grasping examples see [25][4]. The *MATLAB/Simulink* implementation of both simulations and their analyses can be found in the Multimedia Attachment. In the following, we use agents to refer to effectors to highlight their autonomy in contrast to centralized controllers for multi-effector grasping.

We compare the proposed wrench decomposition to the following SoA approaches:

- PM: Point mass approximation [26]
- $G^\dagger$: Moore-Penrose pseudoinverse, e.g. [5]
- G_Δ^+: "Nonsqueezing" pseudoinverse [3]
- VL: Virtual linkage model [17]

Based on the applied wrench $h(t)$ in simulation, we first computed the internal wrench $h_I(t)$ based on the proposed and above SoA wrench decompositions. For the particular simulation scenarios, the proposed wrench decomposition was independent of optimization parameters $s = \{0, 1\}$ and $w \in]0, 1[$. From $h_I(t)$ the proposed measures for disagreement $F_I(t)$, T_I and γ in (28) and (29) were obtained. We furthermore computed the load shares $\alpha_{f,1}$ and $\alpha_{t,1}$ in (25) and the energy shares $\beta_{\text{lin},1}$, $\beta_{\text{rot},1}$ and β_1 in (26) for agent 1[5]. All computations were solely based on the observed $h(t)$, i.e. we assumed not to have any knowledge on a desired trajectory, controllers or load sharing strategies.

A. Shared control of a mobility assistance robot

Let us consider a walker that can actively support an elderly human during walking. Inspired by [21], we examined two scenarios (see Fig. 9):

- the walker (agent 2) generated torque to support the human (agent 1) during turning
- the walker generated opposing forces to avoid an obstacle

1) Computation of applied wrench h: The agents determined the necessary object wrench h_o to track the desired trajectories through a combination of equal inverse dynamics and impedance controllers. We computed the wrench to be applied at the human interaction point based on the reduced Moore-Penrose pseudoinverse $h_{G\dagger 1} = G_1^\dagger h_o$, but then assigned all pure torque to the walker: $t_2 = t_{G\dagger 1}$, $t_1 = 0$. For obstacle avoidance, the walker applied an additional force $f_{\text{obs},2x} = -(\frac{1}{C_{\text{obs}}} - \frac{1}{C_{\text{max}}})\frac{1}{C_{\text{obs}}^2}\dot{p}_o$ when approaching obstacles

---

[4]Although the cost function differs and the force induced torque constraint is missing, we expect qualitatively similar results as in [25] for our proposed wrench decomposition.

[5]We set the load and energy shares to NaN where otherwise meaningless, e.g., $\alpha_{f,1} = $ NaN when $f_o \approx 0$.
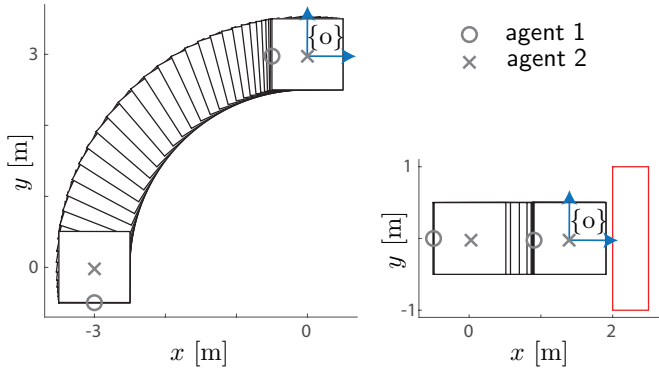
Fig. 9. Walker motion during mobility assistance scenarios: A quadratic nonholonomic walker of length $l = 1\,\mathrm{m}$, mass $m_\mathrm{o} = 25\,\mathrm{kg}$, and moment of inertia $J_\mathrm{oz} = \frac{1}{6}m_\mathrm{o}l^2 = 4.17\,\mathrm{kg\,m^2}$ subject to viscous friction on translation $f_{dx} = -d_\dot{p}\dot{p}_\mathrm{o}$ with $d_\dot{p} = 1\,\mathrm{Ns/m}$ and rotation $t_{dz} = -d_\omega\omega_\mathrm{oz}$ with $d_\omega = 100\,\mathrm{Nm\,s}$. The human (agent 1) interaction with the walker aggregated in one interaction point at $r_1 = [-0.5l\ 0\ 0]$ and the walker (agent 2) applying wrench directly at its CoM. (Left) Walker motion during turning, (right) walker motion during obstacle avoidance. Agent positions at their initial and final positions in gray.

($\dot{C}_\mathrm{obs} < 0$). Obstacle avoidance was active when the distance to the obstacle C_obs (inflated by $0.5l$ of the walker length) was smaller than $C_\mathrm{max} = 2\,\mathrm{m}$.

2) Results collaborative turning: For the collaborative turning task, the agents agreed on the same trajectory p (Fig. 10(a)), while the human (agent 1) applied the necessary forward force f_{1x} (Fig. 10(b)) and the walker (agent 2) the torque t_{1z} (Fig. 10(c)). Fig. 10(d) and (e) show that only the point mass approximation and our proposed optimization yield the correct result of zero disagreement: $F_\mathrm{I} = T_\mathrm{I} = 0$. The pseudo-inverse based methods assume fixed equal load shares on force and torque level. In this case, however, agent 1 took over the complete load share on force level ($\alpha_{f,1} = \beta_{\mathrm{lin},1} = 1$) and agent 2 on torque level ($\alpha_{t,1} = \beta_{\mathrm{rot},1} = 0$ in Fig. 10(f)).

3) Results obstacle avoidance: During the obstacle avoidance scenario, the human (agent 1) intended to move from $p_\mathrm{ox} = 0$ to $p_\mathrm{ox} = 3\,\mathrm{m}$ along the trajectory $p^d_{\mathrm{o},1x}(t)$ displayed in Fig. 11(a). The active obstacle avoidance through counteracting forces f_{2x} stops the walker in front of the obstacle: $p_\mathrm{ox}(t) < p_{\mathrm{obs}x}(t)$. Fig. 11(c) and (d) show the disagreement measures F_I and γ. As for the turning scenario, the point mass approximation and our proposed optimization yield the same F_I. Note that the point mass approximation yields valid solutions for this setup, because the interaction point of the walker coincides with the CoM. The other decomposition methods inflate disagreement F_I due to their underlying assumptions. The peak in disagreement F_I and γ and the switch from $\alpha_{f,1} = \beta_1 = 1$ to 0 (Fig. 11(e)) at $t = 2.1\,\mathrm{s}$ occur when the applied forces of the agents reach equal values: for $t < 2.1\,\mathrm{s}$ agent 1 dominates accelerating the walker, for $t > 2.1\,\mathrm{s}$ agent 2 dominates decelerating the walker.

B. Collaborative object transport

In simulation, two agents transported a beam from a start to a goal configuration in 2D as displayed in Fig. 12 and Fig. 13(a). Thus, a phase of pure rotation was followed by
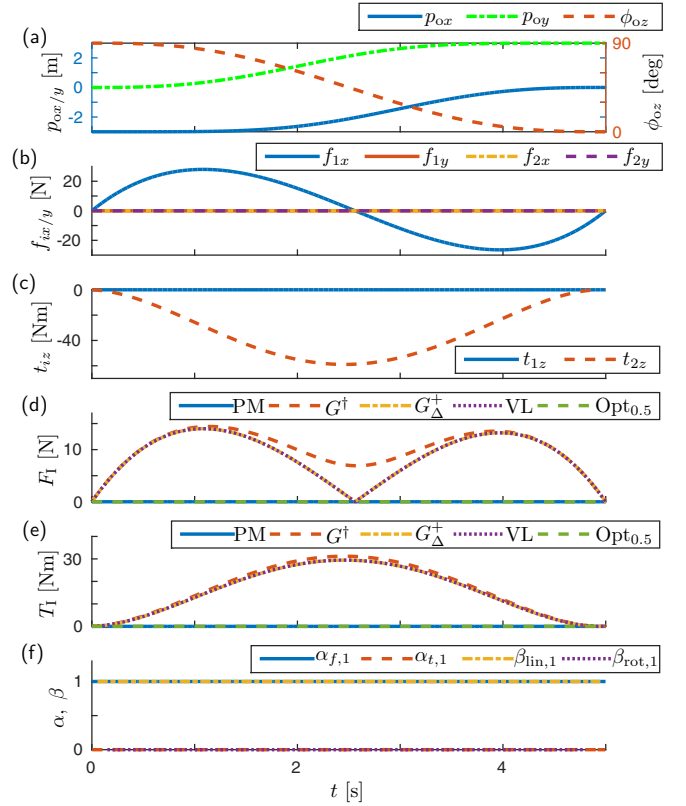

Fig. 10. Analysis of the simulated assisted turning task: (a) Trajectory, (b) applied forces f_{ix}, f_{iy} and (c) torques t_{iz} in the plane by agents $i = 1, 2$, (d) disagreement on force and (e) torque level based on SoA wrench decompositions PM, $G^\dagger$, $G_\triangle^+$ and VL, and our proposed optimization (Opt), (f) load shares $\alpha_{f,1}$, $\alpha_{t,1}$ and energy shares $\beta_{\mathrm{lin},1}$, $\beta_{\mathrm{rot},1}$. Only the proposed wrench decomposition (Opt) and the point mass approximation consistently yield the correct result $F_\mathrm{I} = T_\mathrm{I} = 0$.

a phase of combined rotation and translation, and a phase of pure translation. We furthermore varied how the agents share the load and to which extent forces or torques were applied to induce the required object torque for rotation. Throughout the simulation, the agents agreed on the same trajectory and used the same controller parameters. Thus, we expect the analysis to reveal zero disagreement $F_\mathrm{I} = T_\mathrm{I} = 0$.

1) Computation of applied wrench h: The agents determined the necessary object wrench h_o to track the desired trajectory through a combination of equal inverse dynamics and impedance controllers. The applied wrench was computed from the necessary object wrench h_o based on the parametrized pseudoinverse of [27] for two agents

$$h_{G+M} = G_M^+ h_\mathrm{o} = \begin{bmatrix} m_1^*(m_\mathrm{o}^*)^{-1}I_{3\times3} & m_1^*(J_\mathrm{o}^*)^{-1}S(r_1)^\top \\ 0_{3\times3} & J_1^*(J_\mathrm{o}^*)^{-1} \\ m_2^*(m_\mathrm{o}^*)^{-1}I_{3\times3} & m_2^*(J_\mathrm{o}^*)^{-1}S(r_2)^\top \\ 0_{3\times3} & J_2^*(J_\mathrm{o}^*)^{-1} \end{bmatrix} h_\mathrm{o},$$
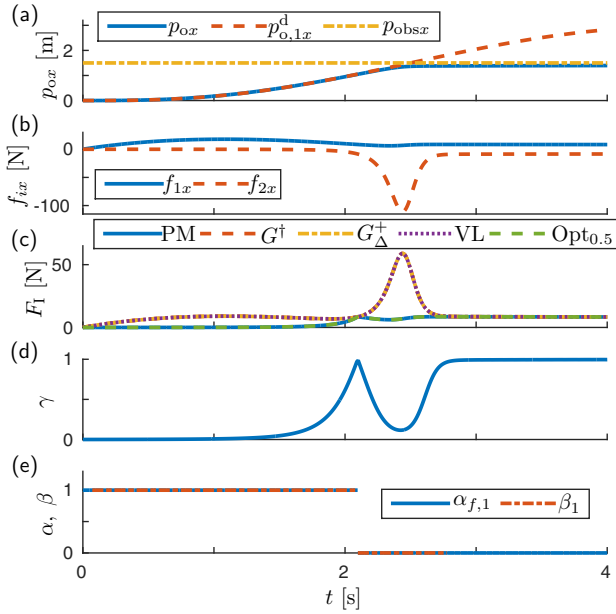(30)

Fig. 11. Analysis of the simulated assisted obstacle avoidance task: (a) Actual p_{ox} and planned $p_{o,1x}^{d}$ trajectory and inflated obstacle border p_{obsx}, (b) applied forces f_{ix} by agents $i = 1, 2$ ($f_{iy} = t_{iz} = 0$), (c) disagreement on force level based on SoA wrench decompositions PM, $G^{\dagger}$, G_{Δ}^{+} and VL, and our proposed optimization (Opt), (d) disagreement γ, (e) load share $\alpha_{f,1}$ and energy share $\beta_1 = \beta_{lin,1}$. High forces required for deceleration in front of the obstacle are interpreted as internal forces by the wrench decomposition methods $G^{\dagger}$, G_{Δ}^{+} and VL.
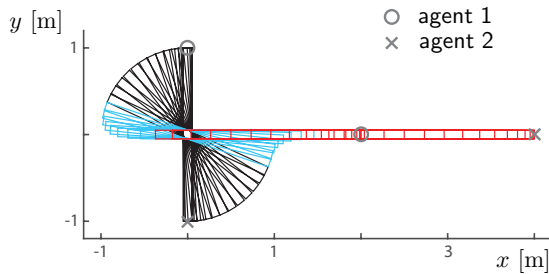

Fig. 12. Beam motion for the simulated 2D transport task: Beam of length $l = 2\,\text{m}$, mass $m_o = 1\,\text{kg}$, and moment of inertia $J_{oz} = \frac{1}{12} m_o l_o^2 = 1\,\text{kg m}^2$, subject to viscous friction on translation $f_d = -d_{\dot{p}}\dot{p}_o$ with $d_{\dot{p}} = 1\,\text{Ns/m}$ and rotation $t_{dz} = -d_{\omega}\omega_{oz}$ with $d_{\omega} = 1\,\text{Nm s}$. Phase of pure rotation (black), followed by phase of combined rotation and translation (blue), followed by phase of pure translation (red). Agent positions at their initial and final positions in gray.

with virtual masses m_i^* and moment of inertias J_i^* with $i = 1, 2$ as parameters, which have to obey

$$m_o^* = \sum_i^{n=2} m_i^*, \qquad (31)$$

$$J_o^* = \sum_i^{n=2} J_i^* + \sum_i^{n=2} S(r_i) m_i^* S(r_i)^{\top}, \qquad (32)$$

$$\sum_i^{n=2} r_i m_i^* = 0_{3 \times 1}. \qquad (33)$$

From the last equality (33) follows $m_1^* = m_2^*$ for a symmetric beam as in Fig. 2 and Fig. 7. We further set $J_1^* = J_2^* = I_{3 \times 3}\,\text{kg m}^2$ and vary m_i^* between $1\,\text{kg}$ and $4\,\text{kg}$ as displayed
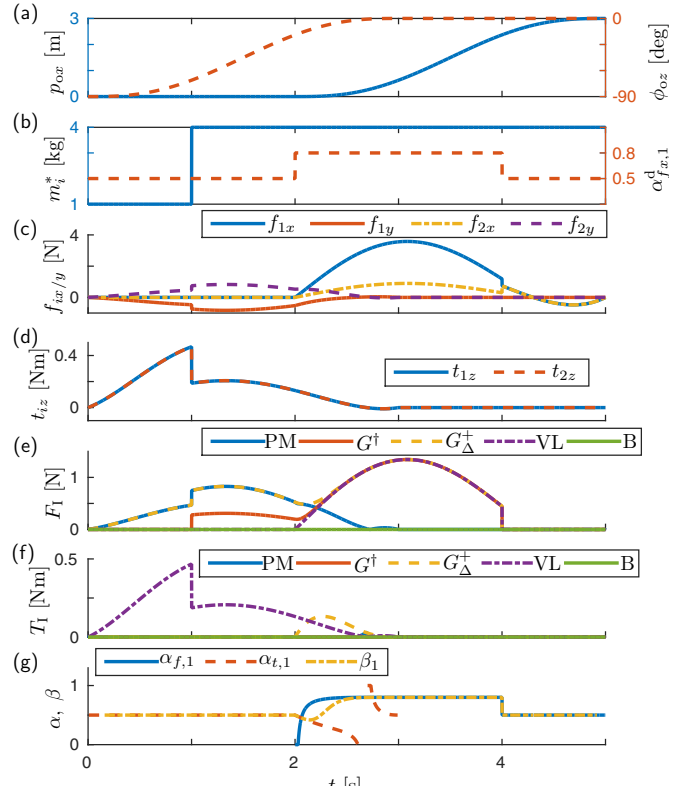

Fig. 13. Analysis of the simulated 2D beam transport task: (a) Trajectory with $p_{oy} = 0$, (b) parameter m_i^* of pseudoinverse [27] and 1D load share $\alpha_{fx,1}$ [8], (c) applied forces f_{ix}, f_{iy} and (d) torques t_{iz} in the plane by agents $i = 1, 2$, (e) disagreement on force and (f) on torque level based on SoA wrench decompositions PM, $G^{\dagger}$, G_{Δ}^{+} and VL, and our proposed 2D beam wrench decomposition (B), (g) load shares $\alpha_{f,1}$ and $\alpha_{t,1}$ and energy share β_1. Only the proposed 2D beam wrench decomposition (B) consistently yields the correct result $F_I = T_I = 0$.

in Fig. 13(b)). Variation of the virtual masses m_i^* regulates to which extent torque $t_{o,i}$ is induced by t_i or f_i. For $m_i^* = 1\,\text{kg}$, the parametrized pseudoinverse G_M^+ is equal to the Moore-Penrose pseudoinverse $G^{\dagger}$, which yields the minimum norm solution for h. For increasing m_i^*, the required torque $t_{o,i}$ is induced to a higher extent through applied force f_i than applied torque t_i.

Due to the restriction on $m_1^* = m_2^*$, the parametrized pseudoinverse G_M^+ cannot be used to design a desired load share but it yields balanced load sharing among the agents. As presented in [8], we varied the desired load share $\alpha_{fx,i}^d$ along the redundant x-direction of the beam (see Fig. 13(b)). This was done by further modifying the x-values $f_{G+M,ix}$ of the computed wrench h_{G+M} from (30) in the null space of the grasp matrix $\text{Ker}(G) = [1 \quad 0_{1 \times 5} \quad -1 \quad 0_{1 \times 5}]^{\top}$ according to

$$h = h_{G+M} + (-f_{G+M,1x} + 2\alpha_{fx,1}^d f_{G+M,1x})\text{Ker}(G). \quad (34)$$

Thus, for $\alpha_{fx,1}^d = 0.5$ we kept $h = h_{G+M}$ and consequently $f_{1x} = f_{2x}$. In contrast for, e.g., $\alpha_{fx,1}^d = 1$ agent 1 would take over the complete load in x-direction.

2) Results: In simulation, the two agents applied the wrench $h(t)$ displayed in Fig. 13(c) and (d) to track the desired trajectory and achieve the desired load share displayed in Fig. 13(a) and (b), respectively. Fig. 13(e) and (f) show the

results for the disagreement F_I and T_I in (28). Our proposed wrench decomposition yields the correct result of zero disagreement between the agents[6]. The point mass approximation proposed in [26] neglects that forces also induce torque for the computation of $f_{\mathrm{M},i}$. As a consequence, opposing forces that were applied to induce torque are interpreted as internal force, which results in $F_\mathrm{I} \neq 0$ during rotation. Wrench decomposition according to the Moore-Penrose pseudoinverse $G^\dagger$ only results in zero disagreement when the agents use $G^\dagger$ to compute h_1 and h_2. This is the case for $m_i^* = 1\,\mathrm{kg}$ during rotation and $\alpha_{fx,i}^\mathrm{d} = 0.5$ during translation. Similar to the Moore-Penrose pseudoinverse-based wrench decomposition, the nonsqueezing pseudoinverse-based wrench decomposition of [3] only yields zero internal force and torque, when $h = G_\Delta^+ h_\mathrm{o}$ holds. For the simulation under consideration, this was only the case during the last second, i.e. pure translation and equal load sharing $\alpha_{fx,i}^\mathrm{d} = 0.5$. Wrench decomposition according to the virtual linkage model of [17] assumes that rotation around the z-axis should be caused by forces instead of torques and interprets any applied torque along z as internal torque. Furthermore, according to the virtual linkage model, internal force only occurs along the x-direction of the beam. Thus, $F_\mathrm{I} = 0$ during pure rotation. However, the virtual linkage model essentially computes the axial force in the center of the beam and assigns its absolute value to F_I, which results in $F_\mathrm{I} \neq 0$ for load distributions $\alpha_{fx,i}^\mathrm{d} \neq 0.5$.

Fig. 13(g) shows the load and energy shares of (25) and (26) for agent 1. The load share $\alpha_{fx,1}^\mathrm{d}$ distributes the demanded object force along the redundant x-direction and is therefore restricted to 1D. Consequently, $\alpha_{f,1} = \alpha_{fx,1}^\mathrm{d}$ only during pure translation. The energy share β_1 combines the force and torque load shares in one measure.

VI. ANALYSIS OF A HUMAN-HUMAN OBJECT TRANSPORT TASK

In this section, we contrast the internal wrench estimated by different decomposition methods during a real pHHI task in order to illustrate how key behavioral measures for pHHI and pHRI are sensitive to a decomposition method. The results will demonstrate our proposed method is more resilient to the inflation of the disagreement index than the others as postulated in the simulation work. Furthermore, we calculate the load share index to characterize the underlying coordination dynamics of the working pair. The coordination dynamics of the working pair was partially controlled by means of a task instruction to the participants. Causes for a non zero disagreement measure during pHHI range from walking motion of the participants, over decision making and to differing intended trajectories.

A. Methods

In this study, 12 pairs of two male participants carried a steel beam (mass $m = 7.7\,\mathrm{kg}$) from a start to a final platform located between obstacles (see Fig. 14). The study was designed to examine how humans haptically reach to

---

[6]The decompositions proposed in [20] and [27] yield zero disagreement as well, but are restricted to 1D or require knowledge of desired velocities with the associated problems outlined in the problem formulation, respectively.
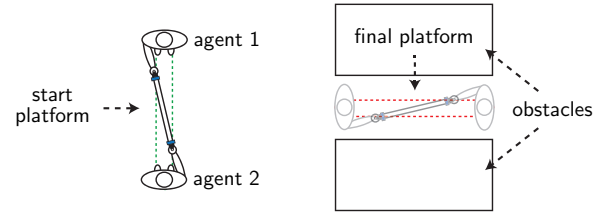

Fig. 14. Experimental setup from a top view: The participants held the beam on the starting platform (green) and moved to the final platform (red) between the obstacles (white boxes).
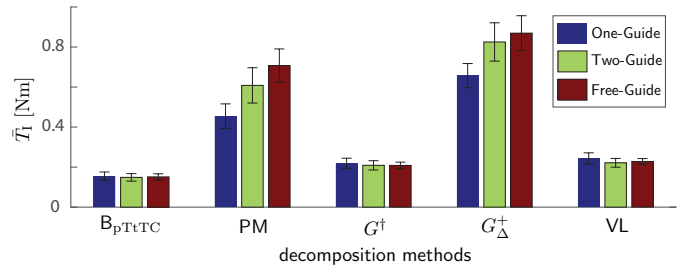

Fig. 15. Average internal torque $\bar{T}_\mathrm{I}$ during the first 600 ms of each trial and agent 1 (leading partner during One-Guide) entering the final platform first: SoA wrench decomposition approaches PM, $G^\dagger$, G_Δ^+ and VL inflate the disagreement measure. Differing guide to disagreement relations ($\bar{T}_\mathrm{I}$(Free-Guide) $>$ $\bar{T}_\mathrm{I}$(Two-Guide) $>$ $\bar{T}_\mathrm{I}$(One-Guide) for PM and G_Δ^+, $\bar{T}_\mathrm{I}$(One-Guide) $>$ $\bar{T}_\mathrm{I}$(Two-Guide) $>$ $\bar{T}_\mathrm{I}$(Free-Guide) for $G^\dagger$ and $\bar{T}_\mathrm{I}$(One-Guide) $>$ $\bar{T}_\mathrm{I}$(Free-Guide) $>$ $\bar{T}_\mathrm{I}$(Two-Guide) for VL and the proposed decomposition) confirm the need for a physically plausible wrench decomposition for interpretable results. The error bar indicates one standard error.

consensus about how to reach the target configuration. Thus, the participants were prohibited from making conversations or intentional communication using their body such as hand gesture.

The experiment was a within-subject design with three levels. The independent variable was the Guiding method. In the One-Guide condition, one of the two partners was assigned the leader role and was always given an instruction about how the beam had to be oriented on the final platform. In the Two-Guide condition, both participants were told about the orientation of the beam at the final platform. In the Free-Guide condition, no instructions were given.

The side at which the participants stood on the platform was counterbalanced and quasi-randomly assigned in each trial. The experimental conditions were block-randomized and the participants performed 10 trials per condition, which resulted in a total of 30 trials per pair. We recorded the applied wrench h using two *JR3* force/torque sensors (JR3, Inc., USA) mounted between the agents' handles and the beam. An *Oqus* motion capture system (Qualisys, Sweden) recorded position and orientation of the beam.

B. Results

1) Disagreement: The beam was kept horizontally during the transportation task. This allowed an application of the efficient 2D beam wrench decomposition implementation introduced in Sec. III-C, which yielded results close to the optimization based solution with $s = 0$ and $w = 0.5$. We observed
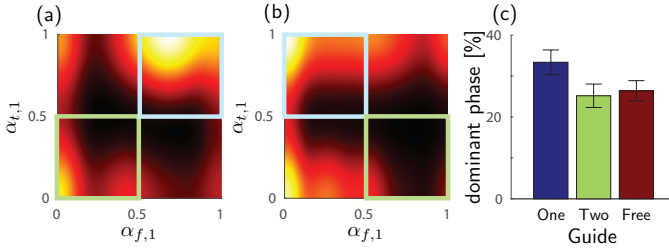
Fig. 16. Force and torque load share pattern based on kernel density estimation with a step size of 0.01 for beam rotation up to 45 deg. (a) Dominant-passive case: force and torque load shares were both high (or low). (b) Specialized case: The load share was selectively high on force or torque, suggesting subtasks (torque vs. force control) had emerged. The example data from a single experimental condition (n = 10) are used to display the results. (c) Percentage of time the joint density of the load share fell in the dominant quadrant. The error bar indicates one standard error.

an inflation of disagreement/compensation on force and torque level for the SoA decomposition approaches, which is in line with our simulation results and the observations for multi-digit grasping in [25]. The experimental setup caused an especially high inflation on internal torque, for which we present a comparison via a repeated-measures ANOVA in the following. The first factor was the Method of decomposition and the second factor was the Guiding instruction. The analysis showing the main effect of Method, $F(4, 44) = 128.39$, $p < .005$, confirming our method to be the most resilient to inflation of disagreement/compensation (Fig. 15). While there was a small effect of Guide ($p = .02$), a clear interaction effect of Method and Guide was found, $F(8, 88) = 3.1$, $p < .005$. Further analysis indicated our disagreement measure is consistent with the amount of guidance information given to the participants such that the largest disagreement was observed in One-Guide ($0.1548\text{Nm} \pm 0.0693$) cases and the smallest in Two-Guide cases ($0.1486\text{Nm} \pm 0.0623$).

2) Load share: Joint density estimation of force and torque load share revealed the coordination strategies of the interacting pairs by large categories into quadrants (see Fig. 16(a,b)). For instance, a participant with high force and torque load share can be classed as a *dominant* partner whereas one with low load share would be classed as a *passive* partner. In contrast, high load on one measure but low on the other indicates a *specialization*, thus each partner was largely responsible for force or torque only. Note that the joint density estimation is always diagonally symmetric between the interacting partners as their share indexes sum to 1: e.g., $\alpha_{f,1} + \alpha_{f,2} = 1$. In this way, we calculated the portion of which agent 1 (the leading partner during One-Guide) is classified into one of the quadrants.

In order to evaluate how the coordination patterns of the load share index was affected by our experimental manipulation, we ran one-way Repeated-measures ANOVA on percentage of time for which the joint density of the force and torque load share fell in the dominant quadrant (Fig. 16(c)). The analysis indicates there is a main effect of Guide on the coordination, $F(2, 22) = 9.219$, $p < .005$. The analysis suggests that the participants formed a dominant-passive coordination strategy more often for One-Guide ($31.39\% \pm 9.99$) than Two-

Guide ($25.20\% \pm 9.49$) or Free-Guide ($26.45\% \pm 8.23$).

VII. DISCUSSION OF LIMITATIONS

A. Uniqueness of the wrench decomposition solution

Wrench decomposition aims at splitting applied wrench into its motion inducing and compensated components. Without further restrictions, infinite decomposition solutions can be found. Pseudo-inverse based approaches find a unique solution by fixing the load shares among the effectors a priori. While this procedure allows for efficient wrench synthesis, it cannot be used to analyze applied wrench, e.g., with respect to load sharing. In this work, we derived physically motivated constraints and formulated wrench decomposition as a convex optimization problem. We showed that the optimization results are in line with solutions proposed in literature, which however only produce physically plausible results for special cases, e.g., [21], [25], [20], [26]. Our approach is the first to yield physically plausible results for general manipulation tasks without assumptions. Only the applied wrenches and the locations of the effector interaction points have to be known. However, the proposed scalarized multi-objective optimization does not yield a unique solution for general manipulation tasks, but depends on the choice of weighting and selection parameters[7]. The multitude of solutions leads us to the conclusion that it is possible to find physically plausible decompositions, but the one and only correct wrench decomposition solution does not exist.

B. Computational cost

The advantage of yielding physically plausible wrench decompositions comes at the cost of having to solve an optimization problem. The optimization is convex and thus can be efficiently solved. We used the *MATLAB* software *CVX*, a package for specifying and solving convex programs [37], [38][8]. The presented analytic solutions for a point mass in Sec. III-A and the "prioritized torque through torque compensation" approximation B_{pTtTC} for the beam transport experiment in Sec. VI yield solutions within less than a ms, and can thus be directly used for realtime haptic interaction control. In contrast, computation of $B_{0.5}$ for the beam transport experiment in Sec. VI required an average time of 0.4 s using CVX with MATLAB R2015a and solver *SeDuMi* v1.34 [39] on a desktop pc[9]. For the general 3D case, the computational cost increased as follows with the number of effectors: $\bar{t}(n = 3) = 0.8\,\text{s}$, $\bar{t}(n = 4) = 1.1\,\text{s}$, $\bar{t}(n = 10) = 2.1\,\text{s}$. Note that CVX is a modeling framework that allows for convenient solving of convex optimization problems written in natural MATLAB syntax, taking over the effort, among others, of transformation into solvable form and the choice of an appropriate solver. Significant speed-up can

---

[7]Note that the problem of weighting does exist for other methods as well. The Moore Penrose pseudoinverse solution ignores this problem by equally weighting the physically distinct quantities force and torque [26].

[8] For the non convex problems, e.g., Fig. 5(c), we used *fmincon* of the *Optimization Toolbox* by *MathWorks*

[9]Processor Intel(R) Core(TM) i5-2500K CPU @ 3.30GHz x 4, no hyper threading, 15.6 GB RAM, ubuntu 14.04 LTS

be achieved by using more efficient commercial solvers [40], [41] and by splitting the solver up into an initialization routine that is performed once and a real-time routine that efficiently solves instances of the same problem [42]. Also, for many interaction scenarios wrench decomposition can be approximated by analytic solutions. Here, we projected the human-human transport task in Sec.VI into the 2D plane and applied the analytic pTtTC solution. Also, for the mobility assistance scenario in Sec.V-A, the point mass approximation as an analytic solution was found.

C. Wrench analysis and wrench synthesis

In this work we focussed on deriving a physically plausible wrench decomposition for the analysis of general manipulation tasks. The proposed wrench decomposition can now be readily applied to pHRI tasks, e.g., to compare different wrench synthesis methods. While we applied different SoA wrench synthesis approaches to control the agents' applied wrench in simulation [27], [21], [8], we refrained from analyzing a real world pHRI task: the added complexity of an uncontrollable human agent and the need for wrench synthesis would impair our goal of fully understanding and evaluating the capabilities of our physically plausible wrench decomposition. Instead, we examined the proposed wrench decomposition on three levels:

- "Snap shots": visually illustrate the method, covering the range of simple 1D to the general 3D cases
- Simulations: allow for controlled disagreement and thus interpretable results
- The pHHI study: exemplifies the application of the derived measures to real world interaction tasks

For wrench synthesis, common pseudoinverse approaches can be straightforwardly applied, if equal load share and a fixed force induced torque to applied torque relation are acceptable. The parametrized pseudoinverse proposed in [27] only partly alleviates above restrictions; i.e. for the beam transport task only the induced torque to applied torque relation was adjustable, while the load share between the agents remained fixed. The null space approach of [8] allows to choose a desired load share along a redundant direction. Nonetheless, their approach is currently limited to 1D, ignoring rotation, with the result of not directly relating to our proposed general load share measures. The derivation of a general wrench synthesis method that achieves a desired load share or controls internal wrench for haptic communication is an interesting and challenging topic that we would like to explore in our future work. Such wrench synthesis applied to robot control will allow more accurate tuning of the robot to the user behavior and intention in pHRI.

VIII. CONCLUSION

The proposed wrench decomposition allows for the first time to separate applied wrench into internal and manipulation wrench for general rigid objects manipulated by multiple effectors, while ensuring physically plausible results. We define manipulation wrench as the wrench with minimum Euclidean norm to produce the resultant object wrench. Physical plausibility is achieved by constraining the internal and manipulation
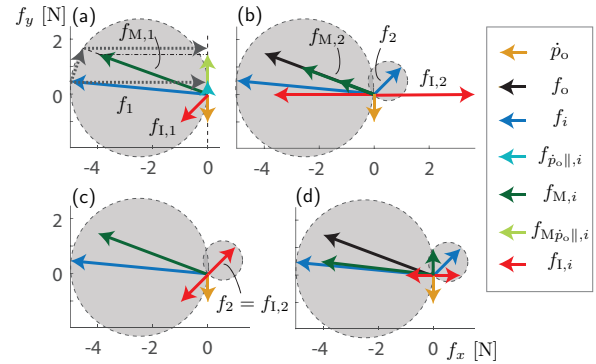

Fig. 17. Effect of work and force constraints: (a) the decomposition of f_1 into $f_{M,1}$ and $f_{I,1}$ adheres to the circular force constraint (9), but not to the work constraint (35) as the projections onto velocity $\dot{p}_o$, $f_{\dot{p}_o\parallel,1}$ and $f_{M\dot{p}_o\parallel,1}$, show that $0 > f_1^\top n \mathrm{d}s > f_{M,1}^\top n \mathrm{d}s$ for $n = \dot{p}_o / \|\dot{p}_o\|$. The gray dotted arrows illustrate that the applied force f_1 and not its projection onto the manipulation force $f_{M,1}$ is relevant for work computations. Optimization results for cost (17) and a point mass $n = 2$ with (b) only work constraint (35), (c) only force constraint (9), (d) work and force constraints (35) and (9).

wrenches by the applied wrench. The proposed optimization is convex and has an intuitive analytic solution for a point mass. The solution for a 2D beam requires optimization only for one special case, which can be approximated through an analytic solution. The efficient 2D beam implementation can potentially be used for real-time control and analysis for various 2-agent object manipulation tasks. Applications in example measures such as load and energy share are defined based on the analytic point mass solution. The extent to which the applied wrench is not used for manipulation, but, e.g., for communication or to express disagreement, can be characterized by the wrench decomposition-based relative cost and Euclidean internal force and torque norms. Simulated mobility assistance and object transport scenarios showed that our method was able to correctly evaluate the control disagreement based on the measured wrench unlike other existing methods. Finally, we illustrated the potential of the derived wrench measures to study aspects as decision making, dominance and specialization during haptic interaction via an exemplary application to a human-human object transport experiment. How to extend the presented wrench decomposition to wrench synthesis that realizes desired load and energy shares or internal wrench for communication remains an open question, which we are interested in examining in future work.

APPENDIX

A. Work vs. force constraints

Schmidts et al. derive the force constraint (9) based on the requirement that a manipulation force $f_{M,i}$ cannot do more mechanical work than the projection of the corresponding applied force f_i onto the manipulation force (see Lemma 1 in [25]). In the following, we show that for work computations, the applied force f_i instead of its projection onto $f_{M,i}$ needs to be considered. Work constraints that ensure that a manipulation force cannot do more work than its corresponding applied force can be formulated as

$$0 \overset{(>)}{\leq} f_{M,i}^\top n \mathrm{d}s \overset{(>)}{\leq} f_i^\top n \mathrm{d}s, \tag{35}$$

$$0 \overset{(>)}{\leq} t_{f\mathrm{M},i}^\top q \mathrm{d}\phi \overset{(>)}{\leq} t_{f,i}^\top q \mathrm{d}\phi, \qquad (36)$$

for an infinitesimal translational displacement $\mathrm{d}n = n\mathrm{d}s \in \mathbb{R}^3$ with $\|n\| = 1$ and an infinitesimal rotational displacement $\mathrm{d}q = q\mathrm{d}\phi \in SE(3)$ with $\|q\| = 1$. However, above work constraints are not equivalent to the circular force constraint (9), as illustrated for an example decomposition in Fig. 17. In order to ensure the work of $f_{\mathrm{M},i}$ is bounded by the work of f_i, the current direction of translational velocity $n = \dot{p}_\mathrm{o}/\|\dot{p}_\mathrm{o}\|$ and rotational velocity $q = \omega_\mathrm{o}/\|\omega_\mathrm{o}\|$ of $\{\mathrm{o}\}$ have to be taken into account. In this work, we refrain from requiring a manipulation wrench to obey work constraints (35) and (36). The resultant object wrench h_o could also be needed to withstand an external force such as gravity, which might come along with zero velocity. Our aim is to use wrench decomposition to analyze the extent to which the wrench applied at the individual effectors h_i effects the resultant object wrench h_o, and how much of it is compensated, independent of the current object velocity. An important result of above considerations is that h, and not h_M, needs to be used to compute energy measures as illustrated in the case of energy share in Sec. IV.

B. Proof of Proposition 1

Proof. Multiplication of the inequalities (9)-(11) with the respective Euclidean norms $\|x_\mathrm{I}\|$ with $x_\mathrm{I} = \{f_{\mathrm{I},i}, t_{f\mathrm{I},i}, t_{\mathrm{I},i}\}$ on both sides and insertion of $\|x_\mathrm{I}\|^2 = x_\mathrm{I}^\top x_\mathrm{I}$ and $x_\mathrm{I} = x - x_\mathrm{M}$ of (5) yields

$$x_\mathrm{M}^\top x_\mathrm{M} \leq x^\top x_\mathrm{M} \qquad (37)$$

with pairs $(x, x_\mathrm{M}) = \{(f_i, f_{\mathrm{M},i}), (t_{f,i}, t_{f\mathrm{M},i}), (t_i, t_{\mathrm{M},i})\}$. Insertion of $x_\mathrm{M}^\top x_\mathrm{M} = \|x_\mathrm{M}\|^2$ and rearrangements yield the constraints (14)-(16). □

C. Proof of Proposition 2

Proof. For a point mass ($t_{f\mathrm{M},i} = 0_{3\times 1}$), the optimization problem (17)-(21) can be solved separately for forces and torques, with analogous results. The Lagrangian for the minimization of manipulation force is

$$L = \sum_{i=1}^n \|f_{\mathrm{M},i}\| + \lambda^\top (f_\mathrm{o} - \sum_{i=1}^n f_{\mathrm{M},i})$$
$$+ \sum_{i=1}^n \mu_i (f_{\mathrm{M},i}^\top f_{\mathrm{M},i} - f_i^\top f_{\mathrm{M},i}), \quad (38)$$

with 3 Lagrange multipliers concatenated in $\lambda \in \mathbb{R}^3$ and n Kuhn-Tucker multipliers $\mu = [\mu_1 \dots \mu_n]^\top \in \mathbb{R}^n$. For $\mu_i = 0$

$$\nabla_{f_{\mathrm{M},i}} L = \frac{f_{\mathrm{M},i}}{\|f_{\mathrm{M},i}\|} - \lambda. \qquad (39)$$

From (39) and because $f_\mathrm{o} = \sum_{i=1}^n f_{\mathrm{M},i}$ we see that every non-zero manipulation force has to point into the same direction as the resultant force f_o

$$\frac{f_{\mathrm{M},i}}{\|f_{\mathrm{M},i}\|} = \frac{f_o}{\|f_o\|}. \qquad (40)$$

A unique solution exists for the special case $f_{\mathrm{M},i}^\top f_{\mathrm{M},i} = f_i^\top f_{\mathrm{M},i}$ for all $i = 1, ..., n$. In this case, the manipulation forces $f_{\mathrm{M},i}$ are equal to the projections of the applied forces f_i onto the resultant force f_o: $f_{\mathrm{M},i} = (f_i^\top f_\mathrm{o}) f_\mathrm{o} \|f_\mathrm{o}\|^{-2}$.

Note that this solution only exists if all f_i projections onto f_o point along f_o. From (40) it follows that $f_{\mathrm{M},i} = 0_{3\times 1}$ if $\mathrm{sgn}(f_i^\top f_\mathrm{o}) < 0$. This is equivalent to force compensation along f_o, with the consequence that a unique solution might not exist for $n > 2$. The family of solutions with equal minimum cost J can be described via (22). The solutions (22) are the global minimum due to the convexity of the optimization problem. □

REFERENCES

[1] L. Bucciarelli, *Engineering Mechanics for Structures.* Dover, 2009.
[2] X. Provot, "Deformation constraints in a mass-spring model to describe rigid cloth behaviour," in *Graphics interface.* Canadian Information Processing Society, 1995, pp. 147–155.
[3] I. D. Walker, R. A. Freeman, and S. I. Marcus, "Analysis of motion and internal loading of objects grasped by multiple cooperating manipulators," *IJRR*, vol. 10, no. 4, pp. 396–409, 1991.
[4] S. Erhart and S. Hirche, "Model and analysis of the interaction dynamics in cooperative manipulation tasks," *IEEE T-RO*, vol. 32, no. 3, pp. 672–683, May 2016.
[5] J. Kerr and B. Roth, "Analysis of multifingered hands," *IJRR*, vol. 4, no. 4, pp. 3–17, 1986.
[6] M. Buss, H. Hashimoto, and J. Moore, "Dextrous hand grasping force optimization," *IEEE Transactions on Robotics and Automation*, vol. 12, no. 3, pp. 406–418, Jun 1996.
[7] C. Passenberg, N. Stefanov, A. Peer, and M. Buss, "Enhancing task classification in human-machine collaborative teleoperation systems by real-time evaluation of an agreement criterion," in *Proc. IEEE WHC*, June 2011, pp. 493–498.
[8] A. Mörtl, M. Lawitzky, A. Kucukyilmaz, M. Sezgin, C. Basdogan, and S. Hirche, "The role of roles: Physical cooperation between humans and robots," *IJRR*, vol. 31, no. 13, pp. 1656–1674, 2012.
[9] K. Reed, M. Peshkin, M. Hartmann, J. Patton, P. Vishton, and M. Grabowecky, "Haptic cooperation between people, and between people and machines," in *Proc. IEEE/RSJ IROS*, Oct 2006, pp. 2109–2114.
[10] R. Groten, D. Feth, R. Klatzky, and A. Peer, "The role of haptic feedback for the integration of intentions in shared task execution," *IEEE Transactions on Haptics*, vol. 6, no. 1, pp. 94–105, 2013.
[11] R. Bonitz and T. Hsia, "Force decomposition in cooperating manipulators using the theory of metric spaces and generalized inverses," in *Proc. IEEE ICRA*, May 1994, pp. 1521–1527 vol.2.
[12] J. K. Salisbury and J. J. Craig, "Articulated hands: Force control and kinematic issues," *IJRR*, vol. 1, no. 1, pp. 4–17, 1982.
[13] Y. Nakamura, K. Nagai, and T. Yoshikawa, "Dynamics and stability in coordination of multiple robotic mechanisms," *IJRR*, vol. 8, no. 2, pp. 44–61, 1989.
[14] T. Yoshikawa and X.-Z. Zheng, "Coordinated dynamic hybrid position/force control for multiple robot manipulators handling one constrained object," *IJRR*, vol. 12, no. 3, pp. 219–230, 1993.

[15] B.-R. Zuo and W.-H. Qian, "A general dynamic force distribution algorithm for multifingered grasping," *IEEE Transactions on Systems, Man, and Cybernetics, Part B: Cybernetics*, vol. 30, no. 1, pp. 185–192, Feb 2000.

[16] V. Kumar and K. Waldron, "Force distribution in closed kinematic chains," *IEEE Journal of Robotics and Automation*, vol. 4, no. 6, pp. 657–664, Dec 1988.

[17] D. Williams and O. Khatib, "The virtual linkage: a model for internal forces in multi-grasp manipulation," in *Proc. IEEE ICRA*, May 1993, pp. 1025–1030 vol.1.

[18] L. Sentis, J. Park, and O. Khatib, "Compliant control of multicontact and center-of-mass behaviors in humanoid robots," *IEEE T-RO*, vol. 26, no. 3, pp. 483–501, June 2010.

[19] T. Yoshikawa and K. Nagai, "Manipulating and grasping forces in manipulation by multifingered robot hands," *IEEE Transactions on Robotics and Automation*, vol. 7, no. 1, pp. 67–77, 2 1991.

[20] R. Groten, D. Feth, H. Goshy, A. Peer, D. Kenny, and M. Buss, "Experimental analysis of dominance in haptic collaboration," in *Proc. IEEE RO-MAN*, Sept 2009, pp. 723–729.

[21] M. Geravand, C. Werner, K. Hauer, and A. Peer, "An integrated decision making approach for adaptive shared control of mobility assistance robots," *International Journal of Social Robotics*, pp. 1–18, 2016.

[22] F. Gao, M. L. Latash, and V. M. Zatsiorsky, "Internal forces during object manipulation," *Experimental Brain Research*, vol. 165, no. 1, pp. 69–83, 2005.

[23] G. Slota, M. Latash, and V. Zatsiorsky, "Grip forces during object manipulation: experiment, mathematical model, and validation," *Experimental Brain Research*, vol. 213, no. 1, pp. 125–139, 2011.

[24] E. Noohi, M. Zefran, and J. L. Patton, "A model for human-human collaborative object manipulation and its application to human-robot interaction," *IEEE T-RO*, vol. 32, no. 4, pp. 880–896, Aug 2016.

[25] A. M. Schmidts, M. Schneider, M. Kühne, and A. Peer, "A new interaction force decomposition maximizing compensating forces under physical work constraints," in *Proc. IEEE ICRA*, May 2016, pp. 4922–4929.

[26] J. R. Medina, T. Lorenz, and S. Hirche, *Considering Human Behavior Uncertainty and Disagreements in Human–Robot Cooperative Manipulation*. Cham: Springer International Publishing, 2017, pp. 207–240.

[27] S. Erhart and S. Hirche, "Internal force analysis and load distribution for cooperative multi-robot manipulation," *IEEE T-RO*, vol. 31, no. 5, pp. 1238–1243, August 2015.

[28] F. E. Udwadia and R. E. Kalaba, "A new perspective on constrained motion," *Proceedings: Mathematical and Physical Sciences*, pp. 407–410, 1992.

[29] K. Reed, J. Patton, and M. Peshkin, "Replicating human-human physical interaction," in *Proc. IEEE ICRA*, April 2007, pp. 3615–3620.

[30] J. Chung, B.-J. Yi, and W. Kim, "Analysis of internal loading at multiple robotic systems," *Journal of Mechanical Science and Technology*, vol. 19, no. 8, pp. 1554–1567, 2005. [Online]. Available: http://dx.doi.org/10.1007/BF03023933

[31] T. Yoshikawa, "Virtual truss model for characterization of internal forces for multiple finger grasps," *IEEE Transactions on Robotics and Automation*, vol. 15, no. 5, pp. 941–947, Oct 1999.

[32] S. Boyd and L. Vandenberghe, *Convex optimization*. Cambridge university press, 2004.

[33] T. Wojtara, M. Uchihara, H. Murayama, S. Shimoda, S. Sakai, H. Fujimoto, and H. Kimura, "Humanrobot collaboration in precise positioning of a three-dimensional object," *Automatica*, vol. 45, no. 2, pp. 333 – 342, 2009.

[34] C. Passenberg, A. Glaser, and A. Peer, "Exploring the design space of haptic assistants: The assistance policy module," *IEEE Transactions on Haptics*, vol. 6, no. 4, pp. 440–452, Oct 2013.

[35] D. Feth, R. Groten, A. Peer, S. Hirche, and M. Buss, "Performance related energy exchange in haptic human-human interaction in a shared virtual object manipulation task," in *Proc. IEEE EHC/WHC*, March 2009, pp. 338–343.

[36] C. Madan, A. Kucukyilmaz, T. Sezgin, and C. Basdogan, "Recognition of haptic interaction patterns in dyadic joint object manipulation," *IEEE Transactions on Haptics*, vol. 8, no. 1, pp. 54–66, Jan 2015.

[37] M. Grant and S. Boyd, "CVX: Matlab software for disciplined convex programming, version 2.1," http://cvxr.com/cvx, Mar. 2014.

[38] ——, "Graph implementations for nonsmooth convex programs," in *Recent Advances in Learning and Control*, ser. Lecture Notes in Control and Information Sciences. Springer-Verlag Limited, 2008, pp. 95–110.

[39] J. F. Sturm, "Using sedumi 1.02, a matlab toolbox for optimization over symmetric cones," *Optimization Methods and Software*, vol. 11, no. 1-4, pp. 625–653, 1999.

[40] "Gurobi optimizer reference manual," 2016. [Online]. Available: http://www.gurobi.com

[41] E. D. Andersen and K. D. Andersen, *The Mosek Interior Point Optimizer for Linear Programming: An Implementation of the Homogeneous Algorithm*. Boston, MA: Springer US, 2000, pp. 197–232.

[42] A. Domahidi, E. Chu, and S. Boyd, "Ecos: An socp solver for embedded systems," in *2013 European Control Conference (ECC)*, July 2013, pp. 3071–3076.

Philine Donner Philine Donner received the diploma engineer degree in Mechanical Engineering in 2011 from the Technical Unversity of Munich, Germany. She completed her diploma thesis on "Development of computational models and controllers for tendon-driven robotic fingers" at the Biomechatronics Lab at Arizona State University, USA. From October 2011 to February 2017 she worked as a researcher and PhD student at the Technical Univerity of Munich, Germany, Department of Electrical and Computer Engineering, Chair of Automatic Control Engineering. Currently she works as a research scientist at Siemens Corporate Technology. Her research interests are in the area of automatic control and robotics with a focus on control for physical human-robot interaction.

Satoshi Endo Satoshi Endo is a postdoctoral research fellow at the Chair of Information-oriented Control at TUM, since 2014. He obtained a PhD in Psychology from the University of Birmingham, UK in 2011. His PhD focused on sensory-motor control of cooperative action, with an extension to physical Human-Robot interaction in cooperative object manipulation. His research interests lie in developing and evaluating behavioural models of a physical interaction between a human and a robot using classical system identification as well as stochastic methods. His research experience spans across many research techniques for analysis and evaluation of human behaviour including biomechanical analysis of human movements and physiological analyses using electroencephalography, electromyography, and functional magnetic resonance imaging.

Martin Buss Martin Buss received the diploma engineer degree in Electrical Engineering in 1990 from the Technical University Darmstadt, Germany, and the Doctor of Engineering degree in Electrical Engineering from the University of Tokyo, Japan, in 1994. In 2000 he finished his habilitation in the Department of Electrical Engineering and Information Technology, Technische Universität München, Germany. In 1988 he was a research student at the Science University of Tokyo, Japan, for one year. As a postdoctoral researcher he stayed with the Department of Systems Engineering, Australian National University, Canberra, Australia, in 1994/5. From 1995-2000 he has been senior research assistant and lecturer at the Institute of Automatic Control Engineering, Department of Electrical Engineering and Information Technology, Technical University Munich, Germany. He has been appointed full professor, head of the control systems group, and deputy director of the Institute of Energy and Automation Technology, Faculty IV – Electrical Engineering and Computer Science, Technical University Berlin, Germany, from 2000-2003. Since 2003 he is full professor (chair) at the Institute of Automatic Control Engineering, Technische Universität München, Germany. From 2006-2014 he has been the coordinator of the DFG Excellence Research Cluster "Cognition for Technical Systems" CoTeSys. Martin Buss is a fellow of the IEEE. He has been awarded the ERC advanced grant SHRINE.